and described the resulting highly siliceous zeolites as 'hydrophobic'.

Adsorption of *n*-hexane in contrast is highly energetic with isosteric heats of adsorption of 16–18 kcal mol^{-1} over a wide range of relative pressure. This range is substantially above the heat of liquefaction of *n*-hexane (7.8 kcal mol^{-1}), and similar to the isosteric heat of adsorption of *n*-hexane on the molecular sieve zeolite X, again illustrating the high dispersion energy interactions in crystalline molecular sieves where the adsorption cavities and pores are $\leqslant$ 10 Å, commensurate with the size of the adsorbed molecule. Consideration of the volume, size and geometry of the void in the silicalite structure (Figs 1–3) and the number and size of *n*-hexane molecules (8.8 molecules per unit cell and 4.5 Å kinetic diameter) shows that the molecules must be highly oriented in nearly linear strings one molecule thick. The fit of *n*-hexane in the channels is near perfect, and *n*-hexane becomes a low entropy highly ordered liquid in the silicalite lattice. Typical adsorption volumes for a variety of molecules on silicalite are given in Table 2.

Stability

Silicalite possesses a remarkable stability for a 33% porous crystal. It is stable in air to over 1,100 °C, and only slowly converts to an amorphous glass at 1,300 °C. It is stable to most mineral acids but reacts with HF similarly to quartz. X-ray emission measurements of the SiKβ band show that the mean Si–O bond energy of silicalite exceeds that of quartz by 0.1 eV, and is essentially the same as for cristobalite. In contrast, the mean Si–O bond energy in aluminosilicate zeolites is substantially less than for quartz[9].

Applications

Thus silicalite may offer practical applications in the clean-up of water contaminated with organic compounds. Traces of methanol, propanol, butanol, phenol, 1,4-dioxane, pentane and hexane have been removed from water. The selectivity of silicalite is nearest to that of adsorbent carbons, but it has the advantage of much higher stability to regenerative commercial processes involving thermal, acid, and oxidative conditions.

We thank T. R. Cannan for his assistance in synthesis and adsorption characterisation, and Union Carbide Corporation for permission to publish this article.

Received 18 November; accepted 30 December 1977.

1. McMullan, R. K., Bonamico, M. & Jeffrey, G. A. *J. phys. Chem.* **39**, 3295 (1963).
2. Barrer, R. M. *Adv. Chem. Ser.* **121**, 1–28 (1973).
3. Perron, G., Desrosiers, N. & Desnoyers, J. E. *Can. J. Chem.* **54**, 2163 (1976).
4. Meisel, S. L., McCullough, J. P., Lechthaler, C. H. & Weisz, P. B. *Chemtech*, Feb., 86 (1976).
5. Merlino, S. *Soc. Italiano di Mineralogia e Petrologia—Rendiconti* **31**, 513–540 (1975).
6. Meier, W. M. in *Natural Zeolites: Occurrence, Properties and Use* (eds Sand, L. B. & Mumpton, F. A.) (Pergamon, Elmsford, New York, in the press).
7. Zettlemoyer, A. C. in *Hydrophobic Surfaces* (ed. Fowkes, F. M.) 13–24 (Academic, New York, 1969).
8. Chen, N. Y. *J. phys. Chem.* **80**, 60–64 (1976).
9. Patton, R. L., Flanigen, E. M., Dowell, L. G. & Passoja, D. E. *ACS Symp. Ser.* **40**, 64–75 (1977).

Radon emanation on San Andreas Fault

Chi-Yu King

U S Geological Survey, 345 Middlefield Road, Menlo Park, California 94025

Subsurface radon emanation monitored in shallow dry holes along an active segment of the San Andreas fault in central California shows spatially coherent large temporal variations that seem to be correlated with local seismicity.

RADON is constantly emanated from the Earth into its atmosphere, normally in minute amounts. Radon emanation is known to be anomalously large on active faults and to show temporal variations related to changing atmospheric conditions and possibly nearby seismic activities[1,2]. To check whether it may show premonitory changes useful for earthquake prediction like those reported for the emanation from deep aquifers[3,4], the US Geological Survey began on 7 May 1975 to monitor subsurface radon emanation in 20 shallow dry holes along an active 60-km segment of the San Andreas and Calaveras faults in central California (stations 1-20, Fig. 1). Here I present some initial results of this experiment and discuss possible explanations.

We used a simple track etch method[5–7] that had been developed for uranium exploration to measure radon emanation: a small piece of plastic film (cellulose nitrate) which is sensitive to α radiation is attached to the inside bottom of a plastic cup (9 cm high, 7 cm aperture). The cup is placed upside down at the bottom of a borehole (10 cm in diameter, 0.7 m deep) to expose the film to the soil gas for 1 week, after which it is replaced by a new cup. The air gap in the cup is sufficient to shield the film from all α particles generated in the soil. As radon and its isotopes are gaseous, however, they may move into the cup to emit α particles close enough to leave tracks in the film. The retrieved film is then chemically etched and the enlarged α-particle tracks in the film within an area of nearly 6 mm^2 are counted under a microscope. The measured track density is then assumed to be proportional to the average radon

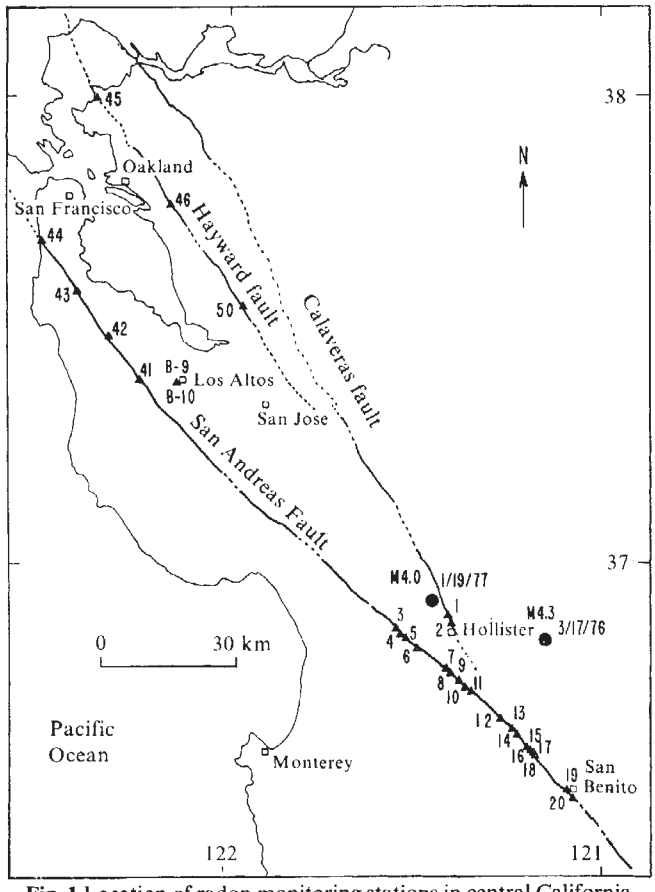

Fig. 1 Location of radon monitoring stations in central California (▲ with station identification numbers) and epicentres of two larger earthquakes (● with magnitudes and dates).

0028–0836/78/0271–0516$01.00

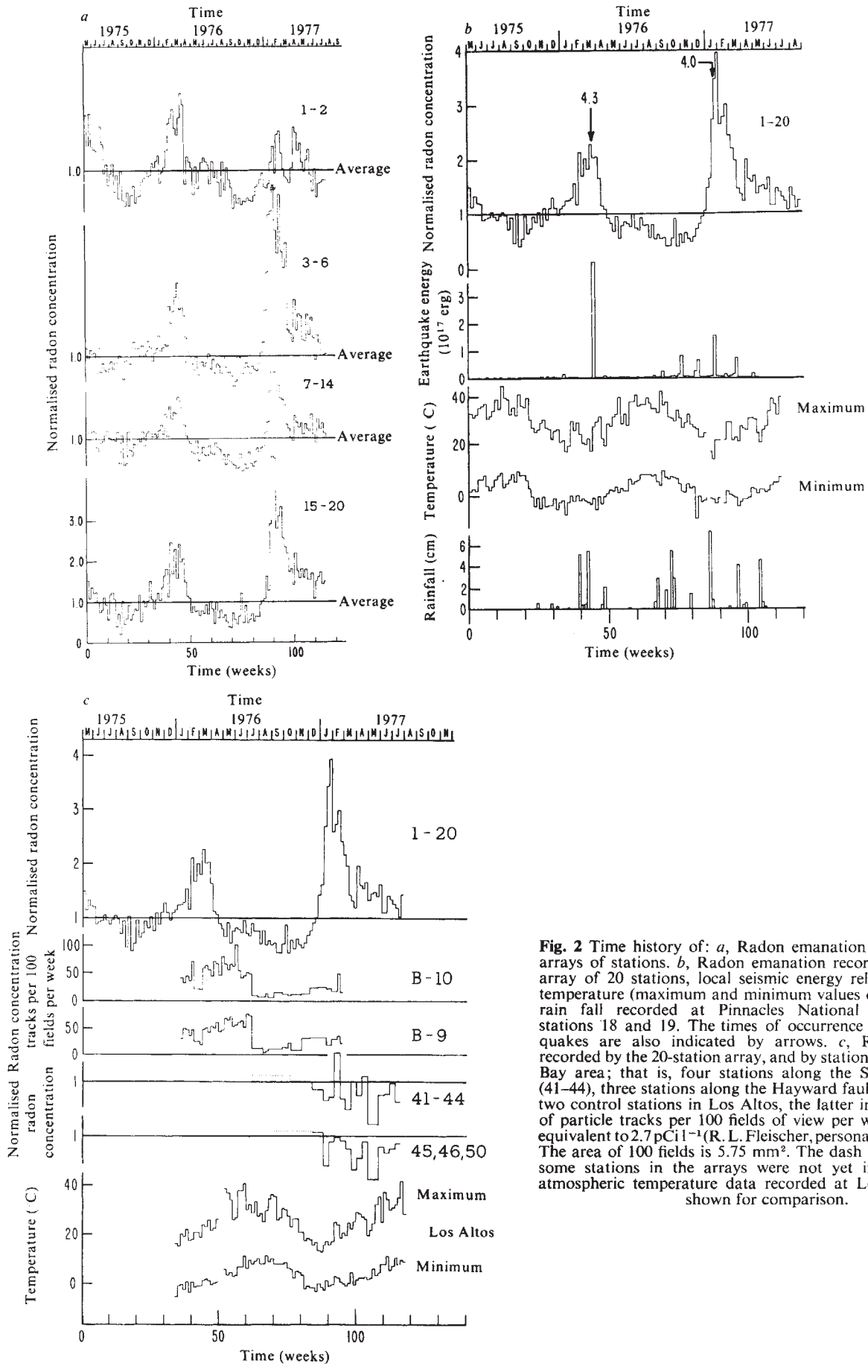

Fig. 2 Time history of: *a*, Radon emanation recorded by four arrays of stations. *b*, Radon emanation recorded by the whole array of 20 stations, local seismic energy release, atmospheric temperature (maximum and minimum values of each week) and rain fall recorded at Pinnacles National Monument near stations 18 and 19. The times of occurrence of the two larger quakes are also indicated by arrows. *c*, Radon emanation recorded by the 20-station array, and by stations in San Francisco Bay area; that is, four stations along the San Andreas fault (41–44), three stations along the Hayward fault (45, 46, 50), and two control stations in Los Altos, the latter in units of number of particle tracks per 100 fields of view per week. Each unit is equivalent to 2.7 pCi l^{-1} (R. L. Fleischer, personal communication). The area of 100 fields is 5.75 mm^2. The dash lines indicate that some stations in the arrays were not yet in operation. The atmospheric temperature data recorded at Los Altos are also shown for comparison.

concentration of the soil gas in the hole during the period of measurement. In the following, I shall not differentiate between the various contributions to the recorded α radiation by radon and by the isotopes thoron and actinon which have much shorter half lives (55 s and 4 s, respectively) than radon (3.8 d).

The boreholes are supported by plastic pipes 0.8 m long. The upper ends of the pipes are approximately 0.1 m above ground surface and are capped to prevent surface water from flowing into the holes and to reduce possible atmospheric effects. A small amount of moisture was sometimes observed on the retrieved films, especially during the springs for these stations, but it does not seem that the moisture has caused any serious detection problems such as reduced sensitivity, since higher radon emanation was recorded during the springs at these stations. The monitoring sites are located mostly in the fault zones for the purpose of maximising possible tectonic signals, because tectonic strain changes are likely to be amplified in a fault zone due to the mechanical weakness of the zone[8].

The measured weekly average values of radon concentration of soil gas ranged from 5 to 2,300 pCi l^{-1}. Figure 2*a* shows radon concentration as a function of time for the 20 stations grouped into four small arrays (stations 1–2 on the Calaveras fault, stations 3–6, 7–14 and 16–20 from north-west to south-east along the San Andreas fault) to improve the signal-to-noise ratio. Data of each array are obtained by first dividing the weekly readings of each station by the average value of the station during the first 40 weeks, and then by summing these 'normalised' values of the same week for all the stations in the array with equal weight.

It is evident from Fig. 2*a* that the measured radon emanation shows large temporal variations that are spatially coherent over long fault segments (≥ 60 km). The radon variations are not correlated with the relatively small amount of rainfall (Fig. 2*b*). Also they do not seem to correlate significantly with barometric pressure changes, presumably because of the integrated nature of the measurement, each value representing a weekly average. But because the two prominent peaks in the radon data are separated by nearly a year (46 weeks), one may suspect a seasonal effect, possibly caused by atmospheric heating and cooling of the ground. As shown in Fig. 2*b*, the correlation between the recorded radon emanation and the atmospheric temperature seems to be exceptionally close. Other observations suggest, however, that this correlation may well be fortuitous. If, for example, the observed temporal radon variations are due mainly to a seasonal effect, one might expect to see fairly similar variations in climatically similar areas, though differences can be caused by different geological conditions at individual sites. Figure 2*c* shows the radon data recorded by stations that were later installed in the San Francisco Bay area (Fig. 1). These include four stations along a 'locked' segment of the San Andreas fault (41–44), three stations along the Hayward fault (45, 46, 50) and two control stations that are only 3 m apart in Los Altos which is about 8 km off the San Andreas fault. The temperature data recorded at Los Altos are also shown in Fig. 2*c* for comparison. The radon emanation there apparently varied quite differently, although the temperature variations are similar to those recorded in the 20-station area.

Figure 2*b* also shows the weekly energy release by earthquakes of magnitude 1.0 and larger within 30 km of the network computed from an energy–magnitude relation given by Richter[9]. The correlation between the radon and the seismicity data seems to be reasonably good. The two largest quakes (magnitude 4.3 and 4.0, respectively, as indicated by arrows in Fig. 2*b* and solid circles in Fig. 1) occurred near the times when the radon emanation reached its peaks. The emanation began to increase rapidly several weeks before the magnitude 4.3 quake when the smaller quakes did not yet increase in number. This result may indicate that the increase in radon emanation is not due to seismic shaking but may possibly be due to strain build up. In contrast, both radon emanation and seismicity increased more or less concordantly during the second 'anomalous' period in which the magnitude 4.0 quake occurred.

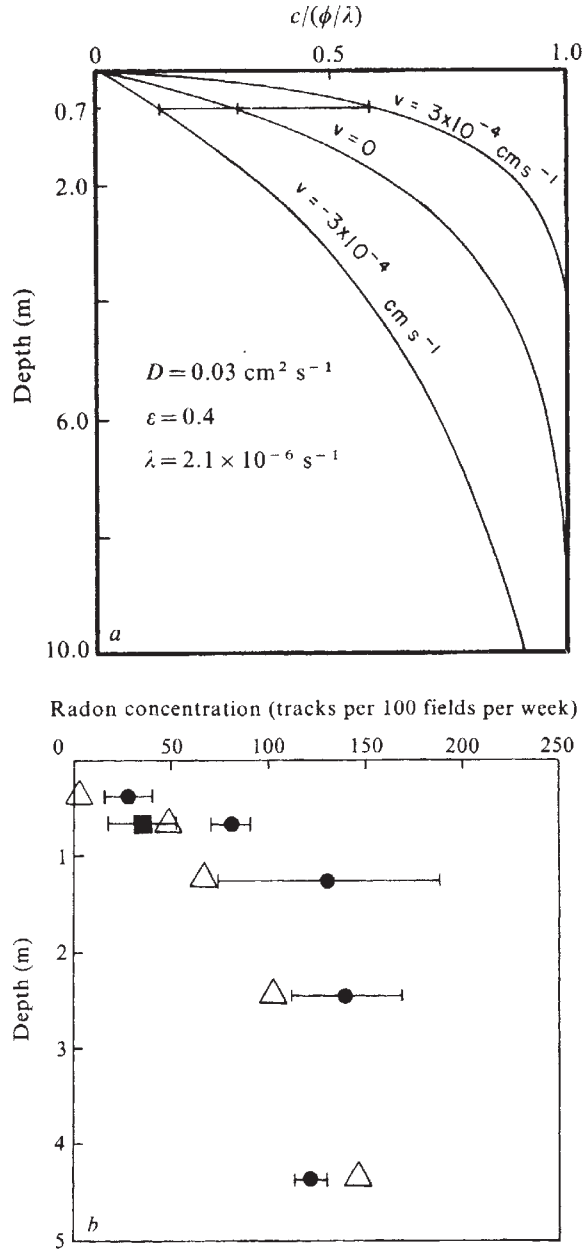

Fig. 3 Radon concentration of subsurface soil gas as a function of depth, *a* for a theoretical model (after Clements[11]); *b*, observed at site 20. The square indicates a long-term average value at the usual monitoring depth of 0.7 m. ●, Indicate the result for an anomalous period (weeks 96–98) and the triangles the result for a nearly normal period (weeks 99–100). The bars indicate 1 σ.

From the available data, I suggest that the observed radon variations are more likely to be related to those of seismicity than atmospheric temperature.

If the observed radon variations are indeed mainly earthquake related, what is the responsible mechanism? In view of the fact that radon has a short half life (3.8 d) and moves slowly in the ground[10], it is unlikely that the detected radon comes from earthquake sources several kilometres deep. The anomalously high radon emanation, however, may conceivably be due to an increase in crustal compression that squeezes out the soil gas in the deep reaching fault gouge zone into the atmosphere at an increased rate, as an increased outgassing rate may perturb the vertical subsurface radon concentration profile (radon concentration is known to increase rapidly with depth by about 3 orders of magnitude), such that deeper soil gas containing more radon is brought up to the detection level. (The proposed

mechanism for earthquake related radon emanation variations will be discussed in more detail elsewhere.)

To obtain some quantitative estimate of the effect of a vertical soil gas flow on radon emanation, let us consider the one dimensional model by Clements[11]. In this model the soil layer is considered to be a homogeneous porous half space (that is the lower boundary is much deeper than 10 m) with uniform radon production. Assume radon migrates vertically by a combination of the following two processes: (1) molecular diffusion governed by Fick's law and (2) gas flow governed by Darcy's law. Having taken into account the equation of continuity for radon and the boundary condition that radon concentration is 0 (negligibly small) at the ground surface, Clements obtained the following steady state result for radon concentration C as a function of depth $(-z)$:

$$C = \frac{\varphi}{\lambda}\left\{1 - \exp\left[\gamma\left(\frac{\varepsilon\lambda}{D}\right)^{\frac{1}{2}}z\right]\right\}$$

where

$$\gamma = \frac{v}{2(\varepsilon\lambda D)^{\frac{1}{2}}} + \left(\frac{v^2}{4\varepsilon\lambda D} + 1\right)^{\frac{1}{2}},$$

φ is radon production rate, λ is its decay constant, ε is soil porosity, D is molecular diffusion coefficient of radon in the soil, and v is apparent soil gas flow velocity (volume of flow per unit time per unit geometric area). This result is shown in Fig. 3*a* for three different flow velocities and some material constants appropriate for typical dry soils. It is evident that a small vertical flow of soil gas (3×10^{-4} cm s^{-1}) can perturb significantly the subsurface radon concentration profile at shallow depths (< 10 m) such that the concentration at the depth of 0.7 m (monitoring depth of this study) is changed by a factor of 2.

To check whether subsurface radon concentration profile varies as predicted, we made radon measurements in boreholes of several different depths separated by several metres at station 20. Figure 3*b*, shows the profiles for a 3-week period (week 96–98) during which the radon emanation was still anomalously high (see Fig. 2*a*), and for a 2-week period (week 99, 100) during which the emanation was nearly back to the average level. It is evident that during the anomalous period radon concentration increased at the shallower depths only, in agreement with the model.

If the observed temporal emanation variations are indeed earthquake related, why are they so large and so spatially coherent for earthquakes that are relatively small? One possibility is that the fault gouge zone, in which most of the radon stations are located, is mechanically much more compliant than the rocks on either side. As a result, strain changes may tend to concentrate in the fault zone over a long segment[8]. Similar spatial coherence is evident in some other fault-zone geophysical data, such as coseismic steps recorded on creepmeters at the times of local earthquakes of comparable magnitudes (> 4.0) (ref. 8) and fault zone deformation episodes indicated by data from alignment arrays[12].

This model may also explain the observed increase in radon emanation resulting from underground nuclear explosions[13].

I thank W. E. Clements, J. Evernden, R. L. Fleischer, J. H. Healy, C. B. Raleigh and J. C. Savage for helpful comments and W. A. Gaman, C. Walkingstick and B. Williamson for technical assistance.

Received 19 September; accepted 15 November 1977.

1. Israel, H. & Bjornsson, S. *Z. Geophys.* **33**, 48 (1967).
2. Okabe, S. *Memoirs of College of Sci., Univ. Kyoto* **28**, 99 (1956).
3. Sadovsky, M. A. *et al. Tectonophysics* **14**, 295 (1972).
4. Group of Hydro-chemistry, the Seismological Brigade of Hobei Province, *Acta Geophys. Sinica* **18**, 279 (1975).
5. Fleischer, R. L., Alter, H. W., Furman, S. C., Price, P. B. & Walker, R. M. *Science* **178**, 255 (1972).
6. Fleischer, R. L., Price, P. B. & Walker, R. M. *Nuclear Tracks in Solids, Principles and Applications* (University of California Press, California, 1975).
7. Gingrich, J. E. *Trans. Soc. Min. Engrs AIME* **258**, 61 (1975).
8. King, C.-Y., Nason, R. D. & Burford, R. O. *J. geophys. Res.* **82**, 1655 (1977).
9. Richter, C. *Elementary Seismology* 366 (W. H. Freeman, San Francisco, 1958).
10. Tanner, A. B. *The Natural Radiation Environment* (eds Adams, J. A. S. & Lowder, W. M.) 161 (University of Chicago Press, Chicago, 1964).
11. Clements, W. E., thesis, New Mexico Inst. Mining Technol. (1974).
12. Harsh, P. paper presented at *Int. Symp. Recent Crustal Movements* (1977).
13. Wollenberg, H., Straume, T., Smith, A. & King, C.-Y. *Lawrence Berkeley Laboratory Rep.* 5905, Univ. California, Berkeley (1977).

Structural comparison of glycophorins and immunochemical analysis of genetic variants

H. Furthmayr
Department of Pathology, Yale University School of Medicine, New Haven, Connecticut 06510

Differences in amino acid sequence of erythrocyte membrane glycophorin A are correlated with M *or* N *blood group activity. A second sialoglycoprotein, glycophorin B, has an amino acid sequence identical to that of glycophorin A*^{N} *in the first 23 positions and carries* N *activity only, suggesting that different structural genes code for the glycoproteins carrying these antigens. Certain genetically variant cells lack glycophorin A, as determined by immunochemical methods, and serological* MN *activity. Other variants lack* MN *activity, but contain normal amounts of glycophorin A in the membrane.*

LANDSTEINER and Levine[1] described a new blood group system in 1927, called MN, in which two alleles *M* and *N* determine the presence of corresponding antigens on the red cells. According to this two-allele theory, three genotypes are possible: *MM*, *MN* and *NN*. In 1947 an additional two-allele antigenic system *Ss* was found[2]; this is closely linked with *MN* and only rarely have recombination events been observed between *MN* and *Ss*[3]. The antigens of the *MN* and *Ss* systems are probably found on different cell surface glycoproteins[4]. There are, however, other data which are inconsistent with this simple genetic interpretation of the serological data. *MM* homozygotes have been shown to express some *N* antigenic activity on the surface of their red cells; this becomes more readily detectable after proteolytic treatment of intact cells[5]. As neuraminidases destroy MN activity of human cells, it has been concluded that carbohydrates and sialic acid in particular are essential in the determinants[6] and that the *MN* alleles code for glycosyltransferases[7,8]. It has, however, also been shown that various reagents reacting with amino groups destroy *MN* activity and this has led to the idea that protein structures are part of the determinants[3,4].

Genetically variant cells have been described serologically, lacking one or the other antigen, and the question arose as to whether absence of the antigen(s) is caused by changes in carbohydrate structure or absence of the glycoproteins carrying the antigenic determinants. We report here studies on the primary structure of glycophorin A isolated from *M* and *N* homozygotes, and the amino terminal segment of glycophorin B. *MN* heterozygotes contain two different glycopeptides in their membrane, which possess different amino acids in positions 1 and 5. The

0028–0836/78/0271–0519$01.00